M. Maslov, A. Boboc, M. Brix, J. Flanagan, M. Romanelli, C. Price and JET contributors

Energy and particle confinement in JET H-mode plasma

Energy and particle confinement in JET H-mode plasma

M. Maslov, A. Boboc, M. Brix, J. Flanagan, M. Romanelli, C. Price

and JET contributors

Energy and particle confinement in JET H-mode plasma

M. Maslov[1], A. Boboc[1], M. Brix[1], J. Flanagan[1], E. Peluso[2], C. Price[1], M. Romanelli[1], and JET contributors*

[1]*United Kingdom Atomic Energy Authority, Culham Centre for Fusion Energy, Culham Science Centre, Abingdon, Oxon, OX14 3DB UK*

[2]*Department of Industrial Engineering, University of Rome "Tor Vergata", via del Politecnico 1, Roma, 00133, Italy.*

Abstract

This work describes the behaviour of the global energy and particle confinement on JET observed in a massive database of H-mode plasmas covering almost whole lifetime of JET operations, both with carbon and metal wall. The analysis is focused on type I ELMy H-modes in stationary phases. It is shown that plasma density in that regime is determined mainly by the plasma current, edge safety factor, triangularity of the last closed flux surface and the hydrogenic isotope mass. That behaviour is consistent for the whole database regardless of divertor configuration or the plasma facing materials. On average, thermal energy confinement time in JET with carbon wall (JET-C) is accurately predicted by the IPB98y,2 scaling. For JET with the ITER-like wall the energy confinement is found to be lower than expected from the scaling. The difference is found to be much stronger in divertor configuration with outer strike point at vertical target and pumping throat at the private flux. Observed lower confinement in JET-ILW can partially be attributed to the additional operational constraints of the metal wall machine, i.e. the avoidance of heavy impurity accumulation via additional gas dosing, but not in full. The isotope effect on the energy confinement in M=1-2 range is found to be the same in JET-C and JET-ILW, thus independent of the wall material, if correlation with plasma density is accounted for. The effect of toroidal magnetic field on the confinement is between zero and slightly negative. Triangularity has generally favourable effect on the energy confinement, but the magnitude changes across the database. Effect of triangularity on plasma density although is always much stronger than on energy confinement, therefore plasmas with high triangularity are in general more dense and colder than at the lower triangularity. The work described in this paper is done under the EUROfusion global confinement database project, and the data shown here will be available to the EUROfusion collaborators shortly. It is also either already a part of the international H-mode confinement database or will be in the future updated version.

1. Introduction

Statistical analysis of the existing experiments is a widely used and relatively inexpensive tool to make predictions of plasma performance in present and future devices. The most known result of such an analysis is the H-mode energy confinement time scaling, also referred to as IPB98(y,2) [1]. It was derived by the international H-mode database working group in 1998, and since then the dataset was expanded further. Presently, 20 years on, a revision of that scaling is on-going based on a much larger dataset [2,3].

Among the 19 tokamaks which supplied the data to the international database, JET is by far the biggest contributor. It provided the largest number of datapoints in a very broad range of plasma parameters, and it is also the tokamak closest to ITER both in geometry and in the plasma facing components, with the ITER-like wall installed in 2011 [4].

JET data had a large influence on the IPB98y,2 scaling and will have an influence on any further scaling derived from the extended dataset. In this work, JET contribution to the international database is carefully analysed. Dependence of the energy confinement time and plasma density on the standard engineering parameters is derived for different subsets of data corresponding to different machine configurations. That includes the standard parameters used in the IPB98y2 scaling, but also others which are not: triangularity of the last closed flux surface and the gas fuelling rate.

This paper is organized as follows. In section 2 the description of the dataset used in this work is given. In section 3, dependence of plasma line averaged density on various engineering parameters is described. Section 4 is dedicated to

the thermal energy confinement time; different regression fits are shown with and without density as one of the parameters. In section 5 comparison of the energy confinement time with IPB98y,2 predictions will be shown for the different subsets, and the differences between JET-C and JET-ILW will be discussed. In section 6 the effect of the SOL density on energy confinement is shown, and in section 7 the summary is given.

2. The JET database.

This work uses three separate sets of data, which belong to different periods of JET operation. The first dataset, referred in this paper as JET-C1, comes from the currently available public version of the international H-mode confinement database [5]. It contains the data from the early period of JET between 1986-2004, which includes the variety of divertor configurations explored at that time [6]. That dataset contains all JET datapoints which were part of the so called DB2v8 dataset used for the energy confinement time study in [1], where the IPB98y2 scaling was derived. In addition to the usual deuterium plasmas, it also contains those with different isotope composition: pure hydrogen, H/D mixtures and the experiments of the DTE1 campaign with 50/50 D/T and close to 100% tritium plasmas.

The second dataset, JET-C2, covers the time period of 2004-2009, which is the later carbon wall JET experiments where the MarkII-HD divertor configuration was implemented. It contains the largest number of datapoints, but no experiments with different isotope masses.

The third dataset covers the whole ITER-like wall period to date – experiments which were done in 2011-2016. The divertor configuration in JET-ILW is identical to MarkII-HD, only the plasma facing materials have changed. That makes JET-ILW and JET-C2 a good matching pair of datasets to study the effect on confinement of the metal versus carbon wall.

JET-C1 database contains data from a large variety of plasmas, therefore the "standard" selection criteria had to be applied in the same way as it is done for the multimachine database [1]. These can be summarized as following:

- Only ELMy H-mode discharges are allowed
- No pellet fuelling used
- Variation in the stored energy is limited to $0.05 < (dW'/dt) / P < 0.35$ to exclude transient conditions
- Total radiated power fraction is below 60%
- Fast particles contribution to the total energy is less than 40%

For the purpose of this work, additional selection was also made:

- Only H-modes with type I ELMs are selected. Entries with ELMs type indicated as "UNKNOWN" and discharge phase as H-mode with giant ELMs (PHASE=HGELM) are also assumed to be type I.
- Entries corresponding to the open Mark0 divertor configuration without cryopump were not included.
- Helium and D/He mixture plasmas were excluded
- Samples where WDIA and WMHD differ by more than 30% were excluded

JET-C2 and JET-ILW samples were already selected from the stationary phases of H-mode plasmas with type I ELMs only, therefore additional selection for that purpose was not required. Plasmas with pellet fuelling, induced TF ripple, induced error field or additional impurity seeding were also excluded from the database. The remaining selection rules were the following:

- Samples where WDIA and WMHD differ by more than 30% were excluded
- Only samples with thermal stored energy exceeding 60% of the total stored energy are considered.
- Only samples with ICRH fast ions energy not exceeding 20% of WDIA are included. This only affected a small number of pulses and is done to limit the errors of the stored energy caused by inaccurate estimation.

The summary of all 3 datasets is shown on table 1.

	Number of samples		I_p, MA	B_t, T	q_{95}	P_{loss}, MW	n_e, m^{-3} $*10^{19}$	LCFS triangularity, δ	M_{eff}
JET-C1	1142	Min	0.69	0.81	2.5	1.01	1.69	0.11	1.02
		Max	4.74	3.97	6.04	24.7	11.4	0.56	2.91
JET-C2	1968	Min	0.811	1.05	2.44	3.54	1.79	0.18	1.86
		Max	4.47	3.57	7.27	27.48	12.04	0.51	2.0

JET-ILW	867	Min	0.97	0.98	2.45	3.3	1.98	0.18	1.0
		Max	3.97	3.79	6.25	32.7	9.93	0.46	2.0

Table 1: Ranges of key parameters in three datasets used for the analysis

3. Plasma density behaviour.

It was shown in [7] that the H-mode plasma pedestal density strongly depends on plasma current, magnetic field and the triangularity at the last closed flux surface. Similar results were reported earlier [8, 9], particularly in relation with the effect of triangularity on plasma density. In this work, the Ordinary Least Square (OLS) regression analysis is done for the plasma line average density dependence on the other engineering parameters, in three datasets separately. LCFS triangularity is used in the form of $(1+ \delta)$ to allow extrapolations to circular plasmas. Particle source S* is used as S*=1+S (1e22 e/s) /n_{GW} (1e19 m^-3), where S is the sum of NBI deposited particles and additional gas dosing, and n_{GW} is the Greenwald density. Similar to the triangularity parameter, unity was added to allow samples with near zero additional particle source to be included in the fit. Results are shown on table 2.

	Const	Ip	B_t	q_{95}	$1+\delta$	P_{loss}	$1+S/n_{GW}$	M_{eff}	R^2
JET-C1	1.28	0.97	-0.217	-	2.09	0.0007	0.72	0.35	0.829
JET-C1	1.83	0.73	-	-0.32	2.08	0.01	0.70	0.36	0.834
JET-C2	1.43	1.15	-0.20	-	2.63	-0.096	0.74	-	0.846
JET-C2	1.84	0.95	-	-0.21	2.62	-0.095	0.73	-	0.846
ILW	1.76	1.34	-0.42	-	2.18	-0.13	0.44	0.38	0.916
ILW	2.84	0.92	-	-0.46	2.25	-0.12	0.42	0.395	0.917

Table 2: exponents for the OLS power law regression fit for <n_e> in three databases.

Scaling expressions for plasma electron density in H-mode plasmas with type I ELMs are consistent across the three datasets. There is a strong correlation between Ip and B_t in each dataset, with the cross-correlation coefficient ranging between 0.8 and 0.9 (see Appendix). This is due to the preference to perform plasma experiments in a small range of q_{95}~Ip/B_t close to 3. Therefore, regression with q_{95} instead of B_t was also performed for each of the datasets, as the correlation between Ip and q_{95} is much weaker. We find similar variation for the exponents of q_{95} parameter between the datasets, and only marginally larger R^2 value for the fits with q_{95} comparing to these done with B_t.

We also performed separate regression fits in two ranges of hydrogenic isotope mass: M_{eff}=1-2 (H and D) and M_{eff}=2-3 (D-T) for the JET-C1 dataset – the only one that contains the whole isotope range. Results are shown on table 3. Plasma density consistently increases with isotope mass in both cases. That trend can also be observed on figure 1, where the residuals of the fit performed without M_{eff} is plotted versus the isotope mass.

	Const	Ip	q_{95}	$1+\delta$	P_{loss}	$1+S/n_{GW}$	M_{eff}	R^2
JET-C1, M_{eff}<2.1	1.85	0.72	-0.33	2.08	0.018	0.70	0.35	0.8313
JET-C1, M_{eff}>1.9	1.80	0.72	-0.33	2.06	0.019	0.70	0.40	0.8075

Table 3: exponents for the OLS power law regression fit for <n_e> in JET-C1, in two groups of hydrogenic isotopes, M_{eff}<2.1 (H+D) and M_{eff}>1.9 (D+T)
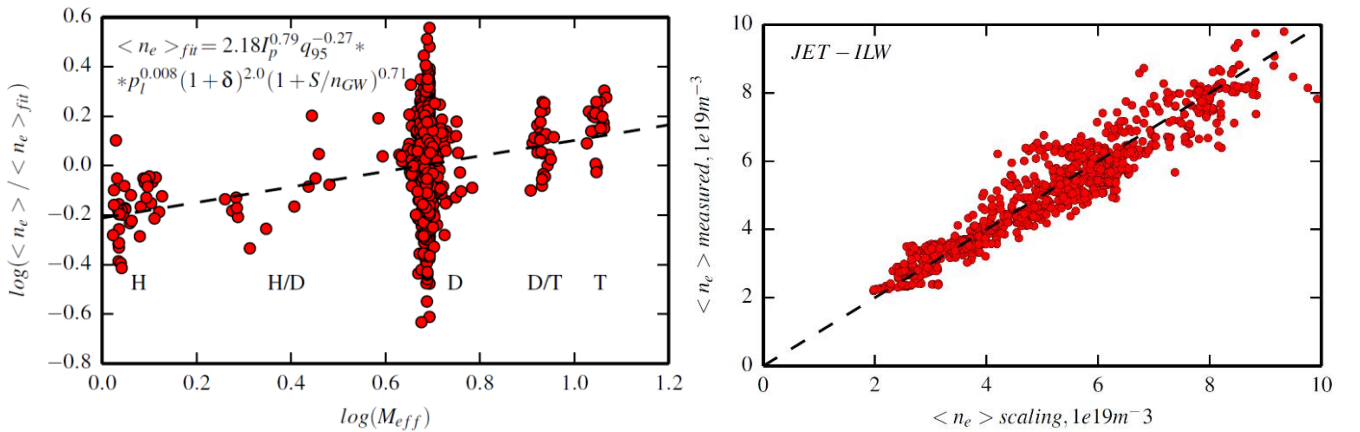

Figure 1a: residual of <n_e> regression fit in JET-C1 dataset performed without M_{eff}, plotted versus log(M_{eff}); 1b) scaling versus measured line averaged electron density in JET-ILW database

In the above regression, the particle source term $1+S/n_{GW}$ is only an approximate estimation of plasma fuelling since it does not include the recycling term, which is not an engineering parameter and also the one which is difficult to quantify. The uncertainty is likely to be larger for JET-C data as the retention of the hydrogenic fuel by the plasma facing materials is a factor of ~10 larger with the carbon wall than in the all-metal wall. Also the relative effect of recycling is larger if additional gas fuelling is low or even zero, which is also characteristic for JET-C plasmas as it will be discussed in section 5. These are probably the underlying reasons for better regression fit of the line averaged density found in the JET-ILW dataset, comparing to JET-C1 and JET-C2. In fact, plasma density can be predicted with much larger confidence than the thermal stored energy in JET-ILW, which will be shown in section 4.

4. Thermal energy confinement time

The definition for the thermal energy confinement time is shown in (1).

$$\tau_{E,th} = W_{th}/P_{l,th} = (W_{dia} - 1.5 * W_{\perp,fast})/(P_{OH} + P_{NBI} + P_{ICRH} - dW_{dia}/dt - P_{cx}) \tag{1}$$

W_{dia} is the total plasma stored energy measured with the diamagnetic loop, $W_{\perp,fast}$ – the gyromotion part of the fast ion energy content, $P_{OH}, P_{NBI}, P_{ICRH}$ are Ohmic, NBI and ICRH heating power deposited in plasma, P_{cx} – the power lost due to charge exchange and first orbit effects. For JET-C1, the values already stored in the database were used, while for the new datasets JET-C2 and JET-ILW they were calculated in a similar manner. $W_{\perp,fast}$ is calculated with the PENCIL code [10] for NBI and PION code [11] for ICRH. Where PION calculations are not available, the ICRH contribution to the fast ion energies was approximated with (2), where P_{ICRH} is the absorbed ICRH power in MW, $n_{e,0}$ is the core electron density, m^{-3} and $T_{e,0}$ is the core electron temperature, eV. (see fig. 2)
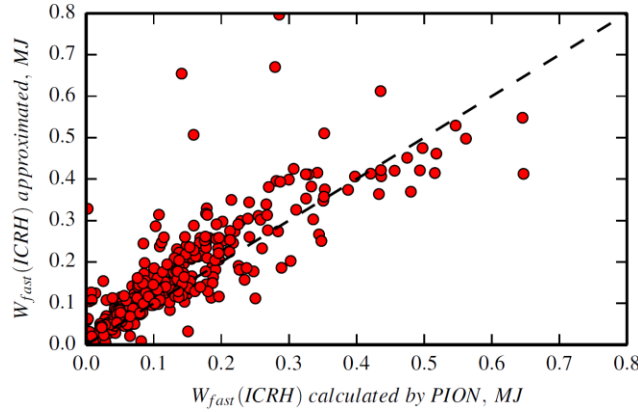

Figure 2: fast ion energy component from ICRH, PION calculation versus approximation (2) in the JET-ILW dataset

$$W_{ICRH,approx} = 0.1 * 10^{14} \frac{P_{ICRH}}{n_{e,0}} T_{e,0}^{1.5} \tag{2}$$

P_{cx} is approximated as $P_{cx} = P_{NBI} * \exp(3.35 - 0.667 * |I_p| - 0.2 * \overline{n_e}) * 0.01$ in all three datasets. It constitutes only a small fraction of P_{loss}, and so this approximation has little influence in the main results of this work.

IPB98(y,2) scaling expression (3) was derived by the ordinary least square method on the power law model. In the JET datasets considered here, variation of the geometry parameters R, k and ε is insufficient for a regression analysis. Therefore, to facilitate the comparison with the results done on the multimachine database, the exponents for these parameters will be fixed to the values from IPB98(y,2), and regression fit for the normalised $\tau^*_{E,th}$, as defined in (4), will be performed instead. Results of the OLS regression applied to the three datasets gives the exponents shown on table 4.

$$\tau_{E,th} = 0.0562 \, I_p^{0.93} \, B_t^{0.15} n_e^{0.41} P_{l,th}^{-0.69} R^{1.97} \kappa^{0.78} \varepsilon^{0.58} M_{eff}^{0.19} \tag{3}$$

$$\tau_{E,th}^* = \tau_{E,th}/R^{1.97}\varepsilon^{0.58}\kappa^{0.78} \tag{4}$$

	Const	Ip	B_t	q_{95}	P_{loss}	n_e	M_{eff}	R^2
IPB98(y,2)	0.0562	0.93	0.15		-0.69	0.41	0.19	-
JET-C1	0.073	1.04	0.11		-0.76	0.31	0.20	0.887
JET-C1	0.0635	1.15		0.12	-0.76	0.32	0.20	0.887
JET-C2	0.0897	1.175	-0.09		-0.63	0.13		0.894
JET-C2	0.095	1.104		-0.055	-0.64	0.13		0.893
JET-ILW	0.059	1.16	-0.22		-0.585	0.08	0.37	0.854
JET-ILW	0.066	0.947		-0.13	-0.59	0.11	0.35	0.844

Table 4: exponents for the OLS power law regression fit for the $\tau_{E,th}^*$ parameters as defined in (4). M_{eff} was not included in JET-C2 regression due to the lack of experiments with isotopes. IPB98(y,2) scaling is shown for comparison.

All three datasets show strong positive correlation with I_p and negative exponent for P_{loss}, consistent with the IPB98(y,2) scaling. The B_t dependence (albeit being rather small) is much less consistent, as it varies between the datasets and even changes sign. Replacing B_t with q_{95} to reduce the cross correlation between the two variables didn't affect the trend significantly. The density exponent in JET-C1 is somewhat lower than derived in the IPB98(y,2) and is significantly lower in JET-C2 and JET-ILW datasets. Exponent for the isotope mass in JET-C1 is similar to the IPB98(y,2), but is almost factor of 2 larger in the JET-ILW, consistent with the observations in the dedicated isotope studies [12]

Regarding the power confinement degradation (exponent for P_{loss}), it should be noted that the dependencies found here and in the IPB98(y,2) database are only valid for a database with a broad variety of parameters and is not reproduced in a dedicated power scan experiments with strong variation of β, as it was shown in [13] and then reproduced in modelling [14]

As it has been shown in section 3, plasma density in these JET experiments is not an independent variable but a strong function of the other engineering parameters. The magnitude of density dependence as calculated in the multiparameter regression therefore affects the exponents for other variables, particularly Ip, B_t and M_{eff}. To demonstrate that, we performed another regression fit for the $\tau_{E,th}^*$, without n_e and with LCFS triangularity 1+δ and particle fuelling 1+S/n_{GW} included, as done in the regression analysis for the density. Results are shown on table 5.

	const	Ip	B_t	q_{95}	P_{loss}	1+δ	1+S/n_{GW}	M_{eff}	R^2
JET-C1	0.068	1.36	0.033	-	-0.74	1.18	-0.155	0.33	0.877
JET-C1	0.068	1.38	-	-0.01	-0.74	1.19	-0.156	0.34	0.877
JET-C2	0.088	1.37	-0.116	-	-0.66	0.67	-0.303	-	0.903
JET-C2	0.098	1.27	-	-0.094	-0.66	0.66	-0.31	-	0.902
JET-ILW	0.066	1.31	-0.28	-	-0.598	0.25	-0.33	0.415	0.874
JET-ILW	0.0836	1.06	-	-0.23	-0.60	0.30	-0.33	0.41	0.870

Table 5: Regression expression with triangularity and particle source instead of the plasma density.

The most significant change in the dependencies after replacing density with 1+δ and 1+S/n_{GW} is observed in the JET-C1 dataset, where the density exponent was the largest. Consistently with the trends shown in table 2, exponents for Ip and M_{eff} have increased, and reduced for B_t (and q_{95}). Exponent for the particle fuelling is negative, which represents energy confinement degradation with increase of the additional gas dosing [9, 15]. Note that the difference in the isotope mass dependence between JET-C1 and JET-ILW in table 5 is reduced, in comparison with the results in table 4. To look deeper into the M_{eff} dependence in the JET-C1, we split that dataset into H/D and D/T subsets, as was done for the density in table 3. The results are shown on table 6. In the range of H/D isotopes, confinement dependence on the isotope mass in JET-C1 is the same as in the JET-ILW, while for the heavier isotope branch D/T the favourable effect is found to be significantly weaker. That can also be seen on fig.3 where log($\tau^*_E/\tau^*_{E,fit}$) where fit excludes the M_{eff} variable is plotted versus log(M_{eff}), in a similar manner as it was done for the density on fig.1
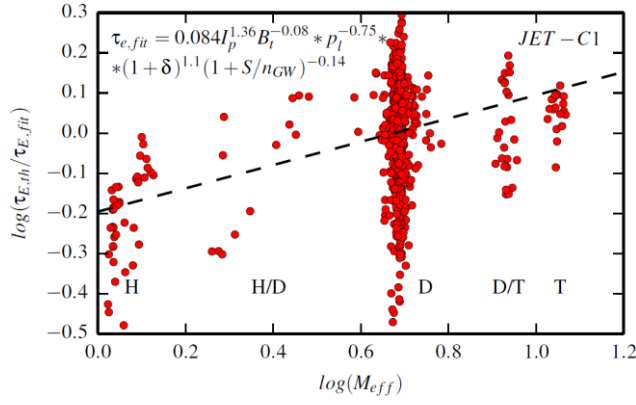
$$\tau_{e,fit} = 0.084 I_p^{1.36} B_t^{-0.08} * p_l^{-0.75} * \\ *(1+\delta)^{1.1}(1+S/n_{GW})^{-0.14}$$

Figure 3: residual of $\tau^*_{E,th}$ regression fit performed without M_{eff}, plotted versus $log(M_{eff})$

	Const	Ip	q95	Ploss	1+δ	1+S/n_{GW}	M_{eff}	R²
JET-C1, M_{eff}<2.1	0.065	1.36	-0.016	-0.73	1.18	-0.18	**0.42**	0.875
JET-C1, M_{eff}>1.9	0.083	1.36	-0.022	-0.73	1.17	-0.17	**0.07**	0.866

Table 6: Regression analysis results for $\tau^*_{E,th}$ in JET-C1 dataset, performed at two different ranges of isotope mass.

Among **1142** data points in JET-C1, **1034** belong to deuterium plasmas ($1.9<M_{eff}<2.1$), and only **108** to the other isotope masses and mixtures (**57** in $M_{eff}<1.9$ range and **51** in $M_{eff}>2.1$ range). Therefore, all the exponents for the main engineering parameters (except the isotope mass) shown on tables 3 and 6 are the same or very similar for both H/D and D/T isotope branches as they are overwhelmingly determined by the deuterium plasmas. In these conditions the isotope mass dependence of the global energy and particle confinement found in this work is only indicative, as it can only be true if dependencies on all other parameters are similar for each isotope, which is not necessarily the case. The only reliable method for establishing the true isotope effect on confinement is observation of the matching pairs of pulses made with different hydrogenic species in otherwise similar conditions. This is only possible in dedicated experiments such as [12] and not in analysis done here or in other similar works based on database statistics.

5. Energy confinement time versus IPB98y,2

Despite differences between IPB98y2 and some individual exponents of the scaling expressions shown on table 4, the thermal energy confinement time in JET-C1 and JET-C2 datasets is very well described by the IPB98y,2 scaling, with the average H98 factor close to 1.0 (see figures 4,5). In the ITER-like wall nonetheless, the energy confinement time is generally below the IPB98y2 predictions (figure 6), which was already pointed out in various publications [16-18].
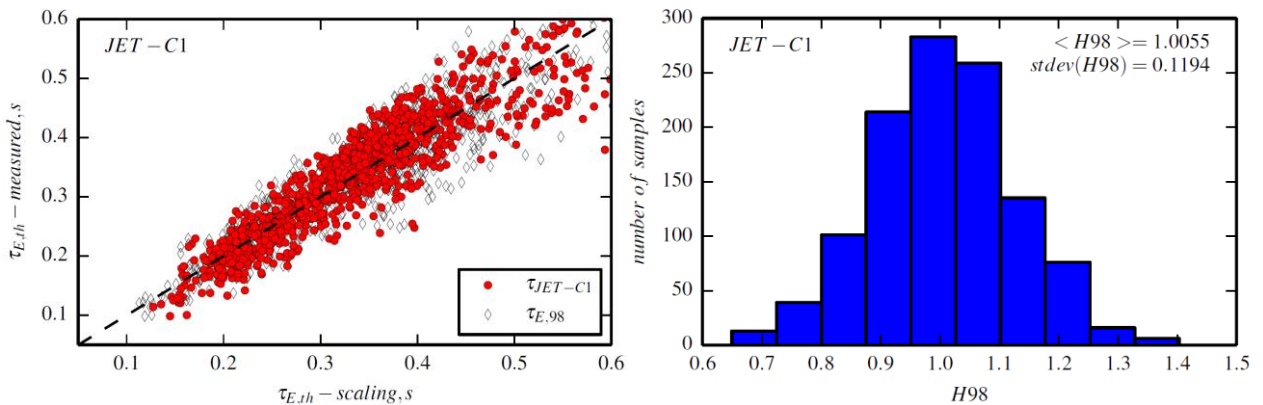

Figure 4 left: thermal confinement time in JET-C1 dataset calculated with the scaling expression derived from JET data (red circles) and from IPB98y,2 expression (empty symbols), versus the experimental value. right: histogram of H98 values for all JET-C1 samples.
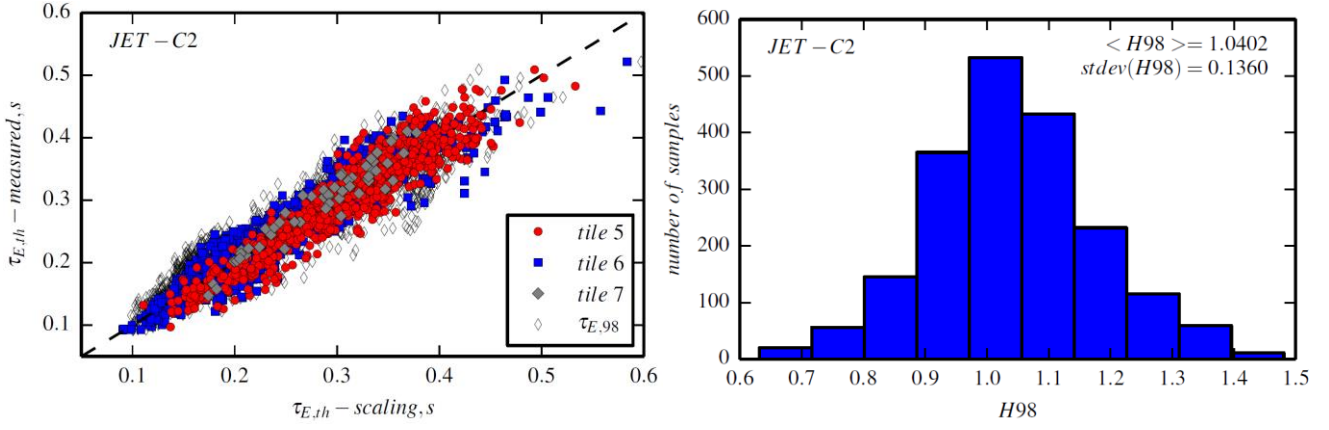
Figure 5 left: thermal confinement time in JET-C2 dataset calculated with the scaling expression derived from JET data (coloured symbols correspond to different divertor outer strike point position) and from IPB98y,2 expression (empty symbols), versus the experimental value. right: histogram of H98 coefficient for all JET-C2 samples.

One of the differences between JET-ILW and JET-C plasmas is that in the presence of the Tungsten divertor, additional gas dosing is always used to avoid impurity accumulation in the core [19]. As it was already mentioned in section 4, additional gas dosing which is an operational requirement in JET-ILW in general causes degradation of the energy confinement, thus contributes to the differences between JET-ILW and JET-C, where H-mode plasmas with naturally low ELM frequency and zero additional gas fuelling were achieved.

On figure 7, H98 versus the gas fuelling parameter S/n_{GW} is plotted for two datasets: JET-C2 and JET-ILW. As one can see, there are very few points at the $S/n_{GW}<0.1$ area in JET-ILW figure, although the same area in JET-C2 is densely populated with average H98 slightly above unity. To compare the carbon wall and metal wall datasets in the same condition, we have recalculated the energy confinement time in the JET-C2 dataset for the datapoints with $S/n_{GW}>0.1$ only. Results of the regression are shown on table 7 and figure 8. While the reduction of the data to the samples containing with additional gas dosing does decrease the average H98 factor down to 0.94, the shortfall in the energy confinement between JET-C and JET-ILW still remains
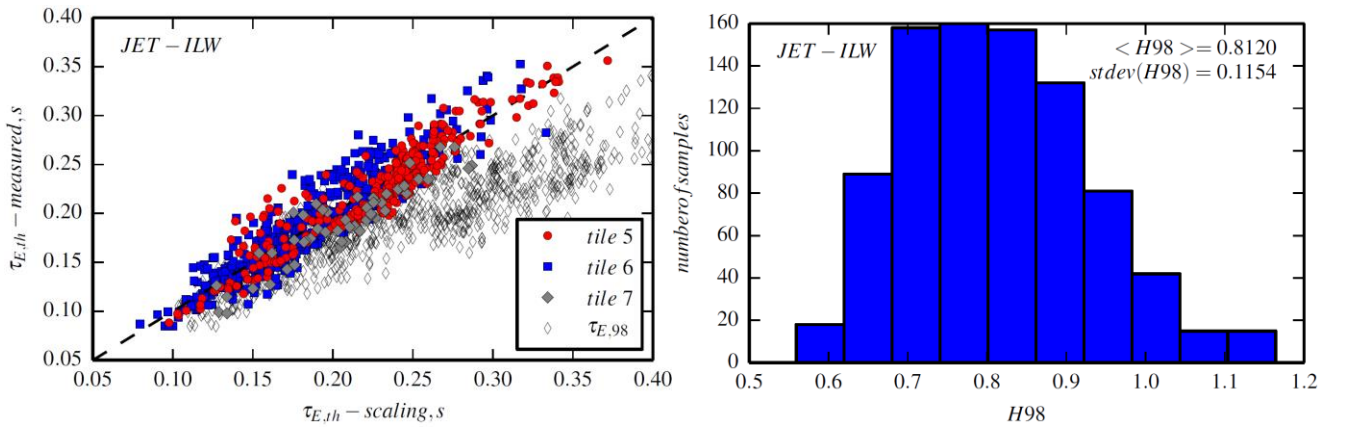

Figure 6 left: thermal confinement time in JET-ILW dataset calculated with the scaling expression derived from JET data (coloured symbols correspond to different divertor outer strike point position) and from IPB98y,2 expression (empty symbols), versus the experimental value. right: histogram of H98 coefficient for all JET-ILW samples.
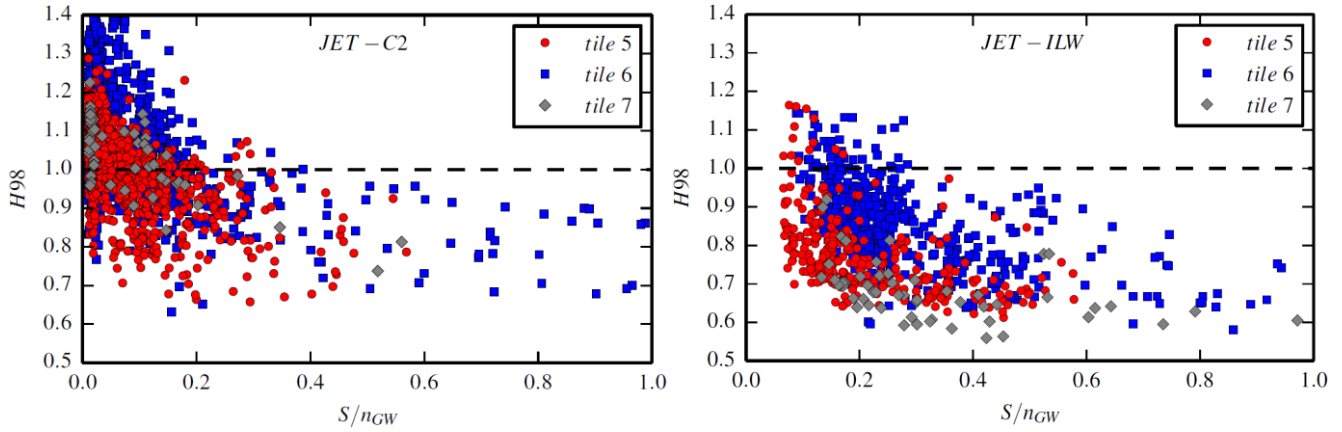
Figure 7: H98 versus normalized particle source in JET-C2 and JET-ILW datasets with different colours corresponding to the different divertor outer strike point positions.
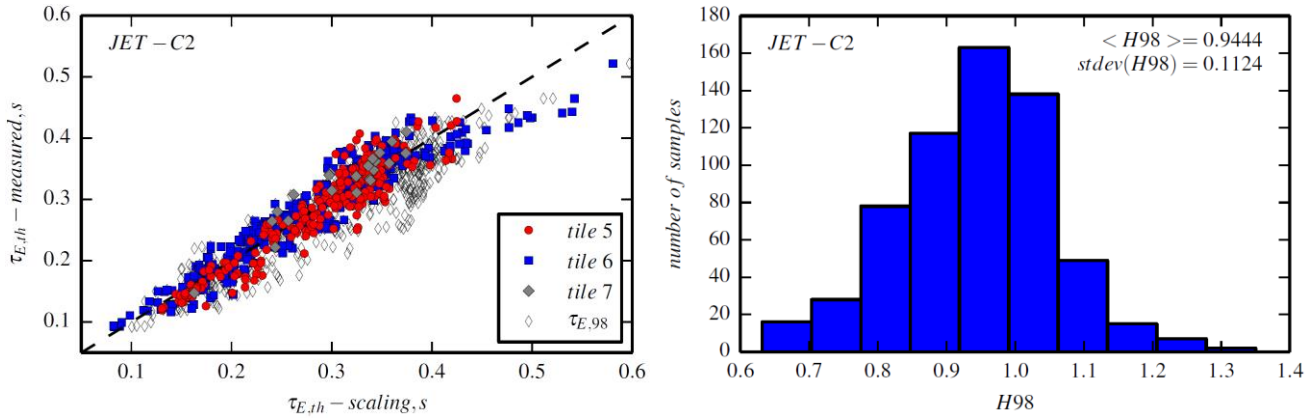

Figure 8 left: thermal confinement time in JET-C2 dataset for the datapoints with $S/n_{GW}>0.1$, calculated with the scaling expression (coloured symbols correspond to different divertor outer strike point position) and from IPB98y,2 expression (empty symbols), versus the experimental value. right: histogram of H98 values.

	N samples	const	Ip	B_t	q_{95}	P_{loss}	1+δ	$1+S/n_{GW}$	R^2
JET-C2	613	0.081	1.52	-0.25		-0.64	0.72	-0.26	0.912
$S/n_{GW}>0.1$		0.115	1.28		-0.28	-0.64	0.695	-0.26	0.909

Table 7: Regression analysis results for $\tau_{E,th}^*$ in JET-C2 dataset, performed for data points with $S/n_{GW}>0.1$ only

In addition to the change in the average energy confinement time, JET-ILW H-mode plasmas also exhibit noticeable dependence of the global energy confinement time on the divertor strike points position ([15,20]). On JET, a set of four in-vessel poloidal field coils is able to create various divertor magnetic configurations, but for simplicity of classification we divide them into three groups only, differentiated by the position of the outer strike point. This normally falls onto JET divertor tiles number 5, 6 or 7 (see figure 9). This configuration is applicable for the Mark2-HD divertor, i.e. for JET-C2 and JET-ILW datasets only. Table 8 shows the confinement scaling factors for JET-C2 and JET-ILW datasets for different divertor outer strike point position. In both cases, JET-C2 and JET-ILW, tile 5 plasmas have reduced confinement than tile 6. This shows up clearly in the H98 coefficient but is less pronounced for the scaling expressions derived in this work.
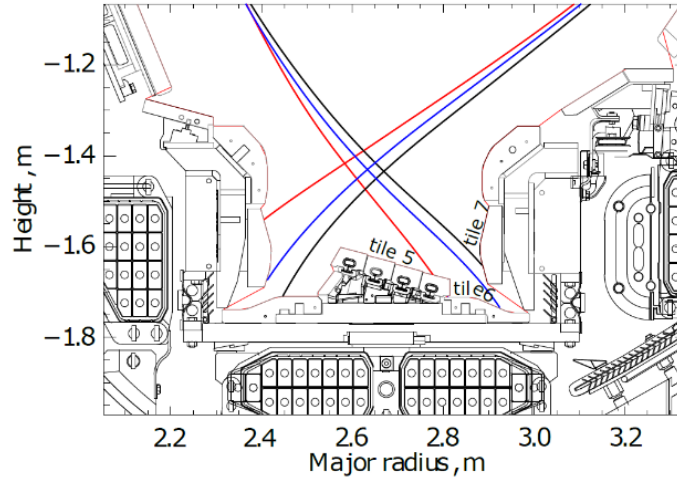
Figure 9: three examples of divertor strike points configurations, with outer leg on tile 5 (red) ,6 (blue) and 7 (black).

			Tile 5	Tile 6	Tile 7
JET-C2	All samples	<H98>	0.99	1.076	1.03
		$<\tau_{scaling}/\tau_{measured}>$	0.98	1.023	1.04
	Samples with S/n$_{GW}$>0.1	<H98>	**0.905**	0.968	0.98
		$<\tau_{scaling}/\tau_{measured}>$	0.98	1.018	1.06
JET-ILW	All samples	<H98>	**0.787**	0.862	**0.688**
		$<\tau_{scaling}/\tau_{measured}>$	0.996	1.02	**0.908**

Table 8: dependence of the H98 factor and the confinement factor derived from the datasets themselves on the divertor outer strike point position.

That can be explained by the stronger effect of the gas dosing on the confinement in tile 5 configurations due to increased recycling [20]. One can also observe it on the figure 7b, where the red points (tile 5) are shifted to the left with respect to the blue points (tile 6), also occupying the area with lower S/n$_{GW}$ where stationary plasmas with outer strike point at tile 6 don't exist.

A noticeable difference in the energy confinement time for tile 7 configurations (strike point on the vertical target, with pumping duct in the private flux) is observed between JET-C and JET-ILW. In all JET-C2 cases shown on table 8, tile 7 configurations had the normalised energy confinement marginally above the other configurations (tile 5 and 6). Nonetheless, in the JET-ILW, tile 7 configurations show the lowest energy confinement for both H98 factor and for the derived scaling. These are grey points on figures 6a and 7b.

6. Energy confinement versus SOL density.

In the previous sections we used additional gas dosing as one of the parameters for the thermal energy confinement scaling. As it was noted, the gas dosing rate itself is not a very suitable parameter to describe the effect, since plasmas with different divertor configurations can have different responses to the same fuelling (e.g. tile 5 versus tile 6 on JET). In addition, the pumping also plays a role. In the datasets considered in this work, all the samples had full divertor cryopump, but plasmas with reduced pumping capability [20] have been demonstrated to have a reduced energy confinement for the same gas dosing rate.

In attempt to account for the recycling and pumping effects on the confinement, we used the scrape of layer density instead of the gas dosing rate as a regression variable. The SOL density was extracted from the Li-beam diagnostic measurements [21]. $n_{e,SOL}$ is defined as plasma density averaged over ρ_{PSI}=1.01-1.03. Position of the separatrix (ρ_{PSI}=1.0) cannot be determined on JET by means of the equilibrium reconstruction to the required accuracy, therefore for the purpose of this work, we assigned the ρ_{PSI}=1.0 position to the pivot point in the profiles at the bottom of the pedestals, where the gradient changes sharply (see figure 11). Note, this definition is different from the one typically used in the pedestal studies [22] where the position of Te=100eV is assumed to be the last closed flux surface. Unfortunately, electron temperature measurements are not available at the location of the Li-beam diagnostic.
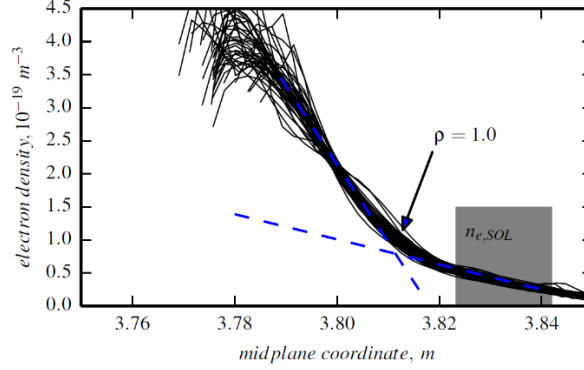

Figure 10: examples of the Li-beam density profiles overlaid, indicating the assigned separatrix position and the area where $n_{e,SOL}$ is measured

Li-beam data on JET is not available routinely, so the analysis had to be done on a significantly reduced dataset of the JET-ILW period only: 238 samples out of 867. On figure 11 we show H98 factor calculated for these samples versus $n_{e,SOL}$ /n_{GW}. In general, the dependence of confinement on $n_{e,SOL}$ is similar to that for the the gas dosing level: higher energy confinement is only possible at low values of $n_{e,SOL}$ and/or low gas dosing. We also note that the tile 5 (red) points on figure 11 are overlapping with blue (tile 6) points, whilst on figure 7b they are shifted with respect to each other, as to achieve the same effect on the confinement and ELMs, plasmas with outer strike point on tile 5 require less gas.

const	Ip	B_t	P_{loss}	1+δ	1+S/n_{GW}	1+$n_{e,SOL}$/n_{GW}	M_{eff}	R^2
0.0657	1.41	-0.357	-0.60	0.23	-0.25		0.39	0.854
0.070	1.38	-0.301	-0.62	0.22		-0.23	0.43	0.865

Table 9: Results of the OLS regression analysis for $\tau_{E,th}^*$ made on the reduced JET-ILW dataset with 237 samples containing $n_{e,SOL}$ data.
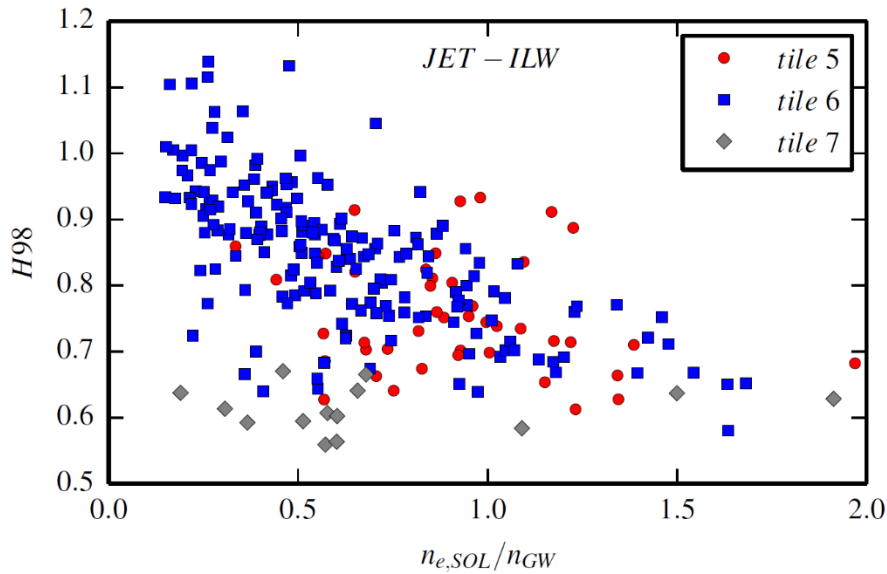

Figure 11: H98 versus $n_{e,SOL}$/n_{GW} for JET-ILW data samples where $n_{e,SOL}$ is available. $n_{e,SOL}$ is in units of $10^{19}m^{-3}$, and n_{GW} is in $10^{20}m^{-3}$

7. Conclusions

In this work we analysed the JET global confinement database covering nearly the whole lifetime of JET operations with ELMy H-mode plasmas. Partly it consists of the data stored in the international H-mode database, which was also the basis for the multimachine energy confinement scaling IPB98y,2. The rest of the database was assembled under the EUROfusion global confinement database project. The international database is currently being extended further and is planned also to include the JET-ILW data described in this work.

We have shown that in JET H-mode plasmas with type I ELMs and gas+NBI fuelling (but no pellets), the electron density scales as a function of the engineering parameters I_p, B_t or q_{95}, LCFS triangularity and the hydrogenic isotope mass (M_{eff}). Density control by additional gas dosing which is required operationally in ILW is inefficient and negatively impacts on confinement.

In this work we've shown separate scaling expressions for plasma density and the energy confinement time derived for the same set of variables. Both regressions have good predictive capability, and in JET-ILW regression for the density even has significantly larger R^2 than for the stored thermal energy. Consideration of the density and stored energy behaviours separately provides a much better insight on the dependence of plasma performance on the individual engineering parameters. For example, increase in plasma current while keeping other parameters the same causes proportional increase in the stored energy, but this mostly comes from increased plasma density at roughly constant temperature, as the I_p exponents in both fits are close. Same applies for the isotope mass dependence. Triangularity generally has a positive effect on the energy confinement with the exponent for $(1+\delta)$ varied between 0.2 and 1.2, but the exponent for the same variable in the density fit is consistently 2.0 or above. Therefore, more triangular plasmas are always denser and colder than the plasmas with low δ.

Large variation of the energy confinement dependence on the triangularity $(1+\delta)$ is consistent with observations done at different times. The strong positive effect was found in the early carbon wall period and reported in [23] – that corresponds to a larger exponent derived from the JET-C1 dataset. From other hand, the effect of the triangularity on the energy confinement was shown to be much smaller or absent with the metal wall [15], which is consistent with a very low dependence derived from the ILW dataset.

In JET with carbon wall, in both datasets considered here, thermal energy confinement time can be quite accurately predicted by the IPB98y,2 scaling expression. Some differences between C1 and C2 datasets do exist in the individual parameters' trends, especially in the density dependence, but the on average the result is not affected. Notably, different density dependence between JET-C1 and JET-C2+JET-ILW is correlated with different dependence of the confinement time on the triangularity.

Experiments with different hydrogen isotopes are present in JET-C1 and JET-ILW datasets. We have shown that the isotope effect on the confinement for $M_{eff}<=2$ range is consistent between JET-C and JET-ILW, if the correlation of the isotope composition with plasma density is accounted for (e.g. by replacing it with the triangularity in the scaling expression). Extending the JET-C1 dataset to T and DT experiments reduces the derived exponent for M_{eff} dependence, since the benefit for the energy confinement appears to be much smaller. At the same time, the effect of the isotope mass on the density is linear and consistent for the whole range of M_{eff}=1-3. Unfortunately, only a handful of experiments with tritium are done at JET so far, and the operational space is poorly explored. More information will be available once the tritium and DT experiments in the JET-ILW will be performed [24]

In JET-ILW, global energy confinement is found to be lower than in the JET-C. This can be partly explained by operational constraints, namely the fact that a certain amount of additional gas dosing is required in JET-ILW H-mode plasmas to control the ELM frequency and mitigate the W accumulation. But the similar levels of gas dosing in JET-C caused smaller confinement reduction than the observed difference between JET-ILW and JET-C, so the rest must be attributed directly to the wall material and/or difference in plasma impurity composition. There is an additional effect on the confinement observed in the JET-ILW, linked to the position of the divertor strike points. Notably, the vertical target (tile 7) configurations with the cryopump throat located in the private flux show reduced confinement in comparison with the other JET-ILW experiments. In the datasets studied here, that behaviour was not observed in the JET-C.

Based on the observation at JET it can be concluded that the IPB98y,2 scaling predictions may overestimate the energy confinement time in future tokamak with Be/W plasma facing component, e.g. ITER. A revision of the multimachine global H-mode confinement scaling is underway [2,3], with one of the main goals to account for the recent results from the metal wall machines and review the extrapolations to larger tokamaks. The updated international database will contain all JET data points discussed in this work.

Acknowledgements

References

[1] ITER Physics Expert Group on Confinement and Transport et al 1999 Nucl. Fusion 39 2175

[2] G. Verdoolaege et al, 27th IAEA FEC, Ahmedabad, India (21-26th October, 2018)

[3] S Kaye et al, 60th Annual Meeting of the APS Division of Plasma Physics, November 5–9, 2018; Portland, Oregon

[4] G F Matthews et al 2011 Phys. Scr. 2011 014001

[5] D.C. McDonald et al 2007 Nucl. Fusion 47 147

[6] JET Team (prepared by R.D. Monk) 1999 Nucl. Fusion 39 1751

[7] H. Urano et al., 42nd European Physical Society Conference on Plasma Physics, Lisbon, Portugal, 22nd – 26th June 2015

[8] L. Horton et al., Nucl. Fusion, Vol. 39, No 1

[9] A. Kallenback et al., Plasma Phys. Control. Fusion 41 (1999) B177-B189

[10] C.D. Challis et al., 1989 Nucl. Fusion 29 563

[11] L.-G. Eriksson et al 1993 Nucl. Fusion 33 1037

[12] C. Maggi et al., Plasma Phys. Control. Fusion 60 (2018) 014045

[13] C.D. Challis et al 2015 Nucl. Fusion 55 053031

[14] S. Saarelma et al., Plasma Phys. Control. Fusion 60 (2018) 014042

[15] C. Maggi et al., Nucl. Fusion 55 (2015) 113031

[16] M N A Beurskens et al 2013 Plasma Phys. Control. Fusion 55 124043

[17] C. Giroud et al 2013 Nucl. Fusion 53 113025

[18] M.N.A. Beurskens et al 2014 Nucl. Fusion 54 043001

[19] I. Nunes et al., Plasma Phys. Control. Fusion 58 (2016) 014034;

[20] P. Tamain et al., Journal or Nuclear Materials 463 (2015) 450-454

[21] M Brix et al., Review of Scientific Instruments 83, 10D533 (2012); https://doi.org/10.1063/1.4739411

[22] E. Stefanikova et al., 2018 Nucl. Fusion 58 056010

[23] G. Saibene et al., Plasma Phys. Control. Fusion 44 (2002) 1769-1799

[24] L. Horton et al., Fusion Engineering and Design 109–111 (2016) 925–936

Appendix

Cross correlation coefficients between logarithms of all used variables for three separate datasets.

JET-C1	Ip	B_t	q_{95}	P_{loss}	$<n_e>$	$1+\delta$	M_{eff}	$1+S/n_{GW}$
Ip	1	**0.922016**	-0.34379	**0.782667**	**0.778107**	-0.10226	0.33575	0.125804
B_t	**0.922016**	1	0.003877	**0.78616**	**0.727643**	-0.02609	0.350057	0.158637
q_{95}	-0.34379	0.003877	1	-0.12506	-0.30774	0.136246	-0.01356	-0.0096
P_{loss}	**0.782667**	**0.78616**	-0.12506	1	**0.721956**	0.142896	0.255172	0.310689
$<n_e>$	**0.778107**	**0.727643**	-0.30774	**0.721956**	1	0.31695	0.339934	0.448538
$1+\delta$	-0.10226	-0.02609	0.136246	0.142896	0.31695	1	-0.10667	0.369183
M_{eff}	0.33575	0.350057	-0.01356	0.255172	0.339934	-0.10667	1	0.043235
$1+S/n_{GW}$	0.125804	0.158637	-0.0096	0.310689	0.448538	0.369183	0.043235	1

JET-C2	Ip	B_t	q_{95}	P_{loss}	$\langle n_e \rangle$	$1+\delta$	M_{eff}	$1+S/n_{GW}$
Ip	1	**0.799243**	**-0.69777**	0.550956	**0.76049**	-0.28133	-0.07211	0.184647
B_t	**0.799243**	1	-0.16099	0.567258	0.58272	-0.16806	-0.14681	0.170587
q_{95}	**-0.69777**	-0.16099	1	-0.23449	-0.58179	0.241927	-0.04535	-0.14377
P_{loss}	0.550956	0.567258	-0.23449	1	0.41001	-0.00255	-0.04629	0.120396
$\langle n_e \rangle$	**0.76049**	0.58272	-0.58179	0.41001	1	0.225681	0.015057	0.431686
$1+\delta$	-0.28133	-0.16806	0.241927	-0.00255	0.225681	1	0.036321	0.138115
M_{eff}	-0.07211	-0.14681	-0.04535	-0.04629	0.015057	0.036321	1	0.096738
$1+S/n_{GW}$	0.184647	0.170587	-0.14377	0.120396	0.431686	0.138115	0.096738	1

JET-ILW	Ip	B_t	q_{95}	P_{loss}	$\langle n_e \rangle$	$1+\delta$	M_{eff}	$1+S/n_{GW}$
Ip	1	**0.916067**	-0.18804	**0.805334**	**0.86571**	0.052035	0.563085	0.139697
B_t	**0.916067**	1	0.211826	**0.78905**	**0.73633**	0.031244	0.584791	0.097684
q_{95}	-0.18804	0.211826	1	-0.02298	-0.2904	0.015978	0.089113	-0.14608
P_{loss}	**0.805334**	**0.78905**	-0.02298	1	0.594271	0.029314	0.375857	0.089157
$\langle n_e \rangle$	**0.86571**	**0.73633**	-0.2904	0.594271	1	0.307417	**0.668526**	0.248304
$1+\delta$	0.052035	0.031244	0.015978	0.029314	0.307417	1	0.109916	-0.12027
M_{eff}	0.563085	0.584791	0.089113	0.375857	**0.668526**	0.109916	1	0.105184
$1+S/n_{GW}$	0.139697	0.097684	-0.14608	0.089157	0.248304	-0.12027	0.105184	1